Reservoir quality and burial model evaluation by kinetic quartz and illite cementation modeling: Case study of Rotliegendes, north Germany

Benjamin Busch, Christoph Hilgers, Robert H. Lander, Linda M. Bonnell, and Dirk Adelmann

ABSTRACT

Silicate reaction kinetics provide a complementary means to other established paleothermal indicators such as organic maturation for evaluating thermal reconstructions. In this study we combine the use of an organic maturation model with kinetic models for quartz and illite cementation to evaluate burial history scenarios for five subsalt wells in lithologically and structurally complex Rotliegendes reservoirs. Models for organic maturation are most sensitive to maximum temperature and provide no direct evidence for the time of peak temperature or the overall duration of high temperatures. By contrast, the kinetics of quartz cementation are much more strongly influenced by the duration of exposure to high temperatures compared with organic indicators. Kinetic models for fibrous illite formation similarly are sensitive to time and temperature and provide predictions for the time of illite formation that can be compared with radiometric dates. Used collectively, these organic and inorganic paleothermal indicators provide improved constraints on thermal evolution compared with conventional approaches. In this study we use these indicators to evaluate two alternative burial history scenarios. Scenario 1 incorporates a hypothesized Jurassic heat flow peak together with significant Late Jurassic deposition and subsequent erosion. Scenario 2 omits the Jurassic heat flow peak and omits the deposition and erosion of the Upper Jurassic. Although both of these scenarios are consistent with organic maturation data, scenario 2 leads to a far better match with quartz cement volumes and fibrous illite K-Ar dates.

AUTHORS

Benjamin Busch ~ *Institute of Reservoir-Petrology, Energy and Mineral Resources Group, RWTH Aachen University, Wuellnerstraße 2, 52062 Aachen, Germany; present address: Structural Geology and Tectonophysics, Karlsruhe Institute of Technology, Adenauerring 20a, 76131 Karlsruhe, Germany; benjamin.busch@kit.edu*

Benjamin Busch is a research associate at Karlsruhe Institute of Technology, Germany. He obtained his master's degree in applied geosciences from RWTH Aachen University with a focus on diagenesis, sedimentology, and structural geology of a reservoir. He has worked on a variety of industry-related projects concerning reservoir quality of siliciclastic hydrocarbon reservoirs.

Christoph Hilgers ~ *Institute of Reservoir-Petrology, Energy and Mineral Resources Group, RWTH Aachen University, Wuellnerstraße 2, 52062 Aachen, Germany; present address: Structural Geology and Tectonophysics, Karlsruhe Institute of Technology, Adenauerring 20a, 76131 Karlsruhe, Germany; christoph.hilgers@kit.edu*

Christoph Hilgers is a professor in the Department of Structural Geology and Tectonophysics at Karlsruhe Institute of Technology, Germany. His main research interests are porous and fractured reservoir rocks as well as process and strategy analyses for the optimum use of reservoirs and storage sites.

Robert H. Lander ~ *Geocosm, LLC, 10 Town Plaza #233, Durango, Colorado 81301; roblander@geocosm.net*

Robert H. Lander is a scientific advisor with Geocosm LLC in Durango, Colorado. His primary research interest is in understanding the controls on diagenetic processes in clastic rocks and using this understanding to develop accurate models of rock properties away from well control and through geologic time.

LINDA M. BONNELL ~ *Geocosm, LLC, 10 Town Plaza #233, Durango, Colorado 81301; lmbonnell@geocosm.net*

Linda M. Bonnell is a scientific advisor with Geocosm LLC in Durango, Colorado. Her main interests are in developing and applying diagenesis models that predict reservoir quality in clastic rocks.

DIRK ADELMANN ~ *Wintershall Holding GmbH, Friedrich-Ebert-Straße 160, 34119 Kassel, Germany; dirk.adelmann@wintershall.com*

Dirk Adelmann is a senior geologist at Wintershall Holding GmbH in Kassel, Germany. He is currently working for the subsurface innovation and technology team mainly focused on new applications in clastic reservoir sedimentology.

ACKNOWLEDGMENTS

Benjamin Busch and Christoph Hilgers kindly acknowledge research funding by Wintershall Holding. We thank Philipp Antrett and Michael Peter Suess (both Wintershall Holding GmbH) for supporting this project. Additionally, we thank Petra David (Wintershall Holding GmbH) and Victoria Sachse (Institute of Geology and Geochemistry of Petroleum and Coal, RWTH Aachen University) for stimulating discussions on burial history reconstructions. Constructive and thorough reviews by Christine M. Skirius, Thomas Taylor, and AAPG associate editor David N. Awwiller improved the final version of this manuscript.

INTRODUCTION

Diagenetic studies are used to establish reservoir quality from core material (Schöner and Gaupp, 2005; Gier et al., 2008). Although such studies are essential for understanding the controls on diagenesis and reservoir quality, they are not in a strict sense predictive. Consequently, forward modeling of diagenetic processes, in concert with rock characterization, has become a focus in hydrocarbon exploration and production as a means to make quantitative reservoir quality predictions for undrilled locations (e.g., Lander and Walderhaug, 1999; Walderhaug, 2000; Walderhaug et al., 2000; Taylor et al., 2004, 2010, 2015; Makowitz et al., 2006; Lander et al., 2008; Ajdukiewicz and Lander, 2010). Such reservoir quality prediction modeling relies on the available knowledge of physical and chemical properties of rocks, kinetics of mineral growth, and reconstructed burial histories.

The burial history reconstruction is commonly based on lithologic and stratigraphic information including rock properties, thickness, distribution, and erosion maps as well as on the maturity of organic material (i.e., vitrinite reflectance) and has successfully been applied to many fields (e.g., Littke et al., 2008; Uffmann and Littke, 2011). However, as shown experimentally by Le Bayon et al. (2012), when exposed to high temperatures and pressures, vitrinite reflectance values plateau within minutes to hours, whereas increasingly higher pressures retard organic maturation. Once this plateau is reached, vitrinite reflectance shows little change with increased time at constant temperature and pressure (Le Bayon et al., 2012). Quartz cement growth, however, is shown to follow kinetic relations that are much more sensitive to the duration of exposure to high temperatures (Walderhaug, 1994, 1996, 2000; Lander et al., 2008). Although a recent study suggests reduced quartz precipitation rates in overpressured sandstones (Meng et al., 2013), it omits critical data needed to evaluate this hypothesis such as sandstone modal compositions, grain size distributions, grain coatings, and fluid overpressure and temperature histories. Other studies show no discernable difference in quartz growth rates derived from hydrostatic and highly overpressured areas within a given stratigraphic unit (Walderhaug, 1994, 1996, 2000; Oelkers et al., 1996; Taylor et al., 2004; Lander et al., 2008). Additionally, quartz cementation models show a remarkable ability to reproduce observed cement abundances in highly overpressured sandstones using kinetic parameters that are similar to those obtained from other hydrostatic reservoirs (Taylor et al., 2010, 2015).

If exposed to a constant temperature over a long period of time, the volume of quartz cement increases nearly linearly with time for sandstones that have significant remaining porosity (Makowitz et al., 2006). In contrast, vitrinite reflectance at constant temperature shows little time dependence after an initial

rapid period of change for temperature T (temperature at the end of heat up) greater than 270°C (518°F) (Le Bayon et al., 2012). Thus, short high-temperature pulses such as those associated with transient fluid flow events (e.g., Sindern et al., 2007) generally may be expected to have a larger influence on vitrinite reflectance (provided the temperature is the maximum historical value) compared with quartz cement volume.

The rate of quartz overgrowth cementation is primarily controlled by the area available for overgrowth nucleation, temperature, and the precipitation kinetics (Walderhaug, 1994, 1996, 2000; Oelkers et al., 1996). The nucleation surface area for quartz overgrowths is a function of the quartz grain abundance and size distribution and generally diminishes in response to the occurrence of grain coatings (Heald and Larese, 1974; Lander and Walderhaug, 1999; Walderhaug, 2000; Ajdukiewicz and Larese, 2012; French et al., 2012). Nucleation surface area also decreases as contact areas between grains increase in association with compaction and as quartz and other cement types fill intergranular pores (Lander et al., 2008).

Two empirical approaches have been used for deriving parameters describing the precipitation kinetics: (1) laboratory experiments (e.g., Rimstidt and Barnes, 1980) and (2) analysis of geological constraints (e.g., Walderhaug, 1994, 1996, 2000; Lander and Walderhaug, 1999; Walderhaug et al., 2000; Lander et al., 2008). Of these approaches the latter has proven to be a far more accurate basis for predrill prediction of quartz cement abundances (Ajdukiewicz and Lander, 2010). An additional factor of significance for the kinetics of quartz growth is the reduction in growth rate that occurs with the progressive development of euhedral crystal faces (Lander et al., 2008). This euhedral effect results in reductions of the surface area normalized rate with diminishing crystal domain size. Thus, the growth rate tends to slow as grain size becomes finer for monocrystalline grains and to be lower for polycrystalline grains compared with monocrystalline grains of comparable size (Waugh, 1970; Lander et al., 2008).

Although previous studies have considered the application of quartz cement abundance as a thermal indicator (Awwiller and Summa, 1997; Lander et al., 1997a, b; Perez et al., 1999; Matthews et al., 2002), in this study we employ an additional inorganic thermal indicator associated with the reaction of kaolinite and a potassium source (assumed to be K-feldspar grains in this study) to form fibrous illite in sandstones (Lander and Bonnell, 2010). The fibrous illitization kinetic model, like the quartz cementation kinetic model, is sensitive to both time and temperature. A difference between these models, however, is that whereas quartz cementation appears to be a continuous process so long as nucleation area is available, the illitization reaction stops once the kaolinite or potassium source is consumed (kaolinite is fully consumed in this study). Additionally, this model has the unique ability to provide predictions for the timing of illite formation that may be compared with K-Ar radiometric dates.

In this study we use diagenetic models to evaluate burial and thermal exposure models of a Rotliegendes reservoir. The burial and thermal models are used to define the pressure and temperature conditions controlling the diagenetic development. By using a well-calibrated diagenetic model based on mineral kinetics and physical and chemical properties of the rocks we test if a given thermal and burial model can reproduce the measured values in quartz cement volumes and illite ages. Additionally, we model the intergranular volume (IGV), porosity, and permeability evolution over time and compare these with core data. These models may improve burial reconstructions that affect organic matter maturation and migration scenarios as well as provide insights into reservoir quality controls, improving play analysis.

GEOLOGICAL SETTING

Samples are taken from five wells penetrating Rotliegendes strata (Bahnsen Sandstone Member, Figure 1) in the North German Basin north of Hannover (Figure 2). Sediments were deposited in fluvioeolian settings within a Permian graben structure and display a wide range of porosities, permeabilities, and cement types. The sampled depositional environments include dunes ($N = 11$), dry interdunes or sand flats ($N = 34$), damp interdunes or sand flats ($N = 4$), and one lacustrine sample ($N = 1$). The Rotliegende is overlain by Zechstein salt layers, and one of the five wells penetrates the Rotliegende strata underneath a salt pillow. All five wells are within a radius of 5 km (3.1 mi) from well C (Figure 2). The reservoirs are currently at depths ranging from 4264 to 4570 m (13,990 to 14,993 ft) true vertical depth.

Authigenic illite samples from Rotliegendes strata of the North German Basin dated using the K-Ar method yield ages of 190–155 Ma (Zwingmann et al., 1998) and approximately 190 Ma (Platt, 1993). Samples originate from core material of wells in a nearby graben setting with present burial depths of Permian and Carboniferous rocks between 4580 and 5280 m (15,026 and 17,323 ft) (Zwingmann et al., 1998, 1999). Detailed information on the unit where samples originate from is not available (Zwingmann et al., 1999). Burial reconstructions for the referenced area are very similar to the studied area (cf. figure 9 in Zwingmann et al., 1999).

BURIAL MODELS

A one-dimensional (1-D) paleothermal history (scenario 1) taken from the work of Peisker (2013) was constrained by only vitrinite reflectance data and present-day temperatures (Figure 3A, B). Vitrinite reflectance calibration was performed by applying EASY%R_o (Burnham and Sweeney, 1989) kinetic models. This model matches the continuous changes in chemical composition of vitrinite, as a response to increasing temperatures during burial, with the optical reflectance of this maceral (Burnham and Sweeney, 1989). This scenario matches vitrinite reflectance data by including a large temperature spike during the Jurassic, reaching maximum temperatures of approximately 220°C (428°F) in the Rotliegende strata of well A and 196°C (345°F) in well B, as well as a second period of high temperatures during the Paleogene (Figure 3B). In scenario 1, temperatures for well C are lower compared with the other study wells because of the expected thermal effect of the overlying salt pillow.

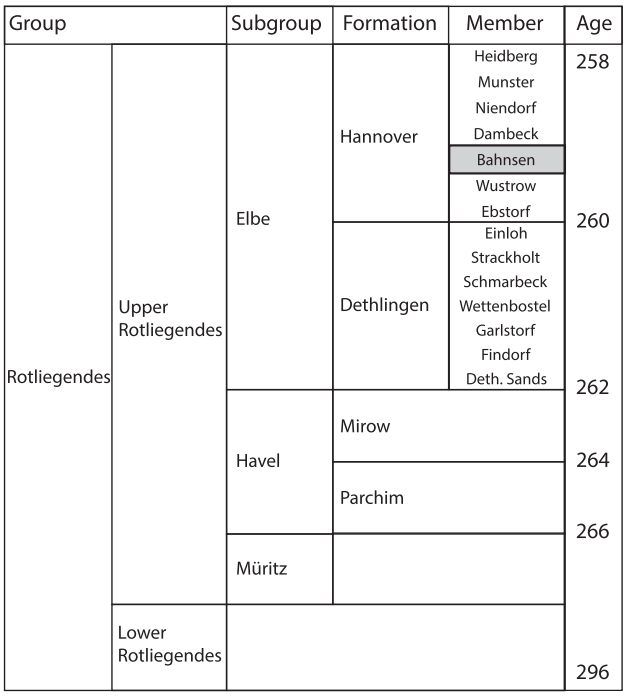

Figure 1. Stratigraphic subdivision of the Rotliegende in north Germany (after Schöner, 2006; stratigraphic ages from Menning, 1995). The Bahnsen Sandstone Member, which is the focus of this study, is part of the Hannover Formation. Deth. = Dethlingen.

Scenario 1 considers heat flow pulses associated with four extensional phases during the (1) Lower Triassic, (2) Upper Triassic, (3) Middle Jurassic, and (4) Upper Jurassic based on general reconstructions for the Southern Permian Basin (Figure 4, heat flow scenario 1) (Pharaoh et al., 2010). The heat flow values for this reconstruction are based on general values from Allen and Allen (2005). The values used for the beginning of the Permian are associated with basin formation and early Permian volcanism (Peisker, 2013). The heat flow increase during the Jurassic (~190 Ma) is associated with deposition following North Sea rifting and is interpreted to be additionally controlled by North Sea doming (cf. Pharaoh et al., 2010). Between rifting events the heat flow decreases to approximately 60 mW/m^2 to attain typical continental heat flow values (Peisker, 2013). The decline in heat flow from the Eocene onward is assumed to match present-day temperatures and heat flow of approximately 55 mW/m^2 (Peisker, 2013).

Based on assumptions regarding vitrinite reflectance development, 700 m (2296 ft) of Late Jurassic deposition and erosion were presumed to have occurred in the study area on the Pompeckj Block to account for the measured vitrinite reflectance data (Peisker, 2013). The thickness of eroded sediments is based on correlations of deposition within the adjacent Lower Saxony Basin (Peisker, 2013), which was not affected by Late Jurassic uplift. A similar thickness of approximately 650 m (2133 ft) of Lower and Middle Jurassic strata was inserted and eroded in models for a nearby region (cf. Schwarzer and Littke, 2007). Sediment deposition resumed in the study area during a marine transgression in the Albian. A period of erosion during the Upper Cretaceous and early Paleogene inversion is represented by the incomplete development of Upper Cretaceous strata.

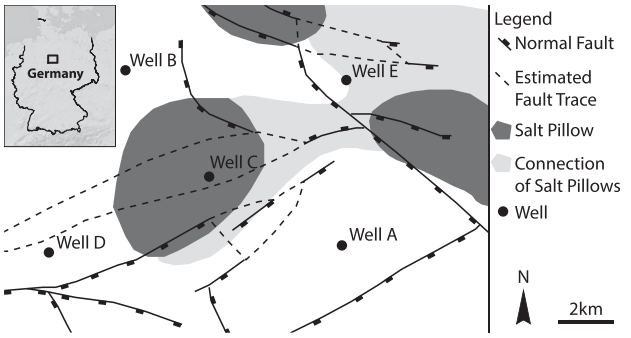

Figure 2. Locations of the five studied wells, including the locations of salt pillows and faults. The dashed lines indicate inferred normal faults.

A second set of 1-D burial history thermal models (scenario 2) was prepared for this study (Figures 3, 4). These lower-temperature models feature a heat flow scenario derived from 1-D, two-dimensional, and three-dimensional burial models published in Schwarzer and Littke (2007) and Uffmann and Littke (2011).

The reconstruction is characterized by a decrease in heat flow following Permian rifting and volcanism to attain a typical continental heat flow of approximately 60 mW/m^2, which is further reduced to 55 mW/m^2, to match present-day values and temperatures on the Pompeckj Block (Figure 4) (Schwarzer and Littke, 2007; Uffmann and Littke, 2011; Bruns et al., 2013). The heat flow reconstructions in the region following Permian rifting feature a decrease to a typical continental heat flow in the Mid-Jurassic, assuming gradual cooling from theoretical stretching models (McKenzie, 1978; Schwarzer and Littke, 2007). The effect of North Sea doming and rifting on the heat flow was neglected because of the distance from the studied area and absence in other models of the region (Schwarzer and Littke, 2007; Uffmann and Littke, 2011). The temperature increase is thus not as large as that modeled in scenario 1. The maximum temperature reached in scenario 2 is 172°C (342°F) and was attained during the phase of deepest burial during the Paleogene. By contrast, in scenario 1 the maximum temperature occurred during the Jurassic. The vitrinite reflectance data and present-day temperature results from scenario 2 provide a match to measured values comparable to that of scenario 1 (Figure 3A, B). The higher temperatures in scenario 1 resulting from the heat flow peak during the Jurassic are not necessary to match the maturity of organic matter (Figure 3A). Scenario 2 does not include the deposition and subsequent erosion of a large sedimentary section during the Upper Jurassic as assumed in scenario 1. Instead, scenario 2 assumes an extended depositional hiatus until the Albian transgression where Lower and Middle Jurassic strata are still present. A localized erosive event during the Upper Jurassic as presented in Schwarzer and Littke (2007) was added to match the presence or absence of Lower and Middle Jurassic strata in each well (cf. Baldschuhn et al., 2001; Bombien et al., 2012).

METHODS

Modal compositions were established from point counting (300 counts) petrographic thin sections and

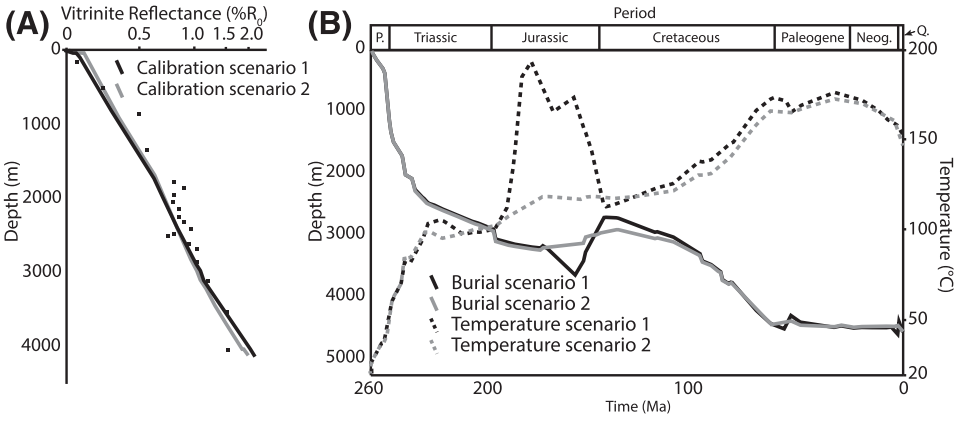

Figure 3. (A) Vitrinite reflectance modeled with EASY%R_o for two subsidence scenarios in PetroMod 2012 and vitrinite reflectance data for calibration from Peisker (2013). The overall modeled results for vitrinite reflectance are similar for the two scenarios. (B) The comparison of two burial scenarios for well B highlights the small difference in burial depth reconstructions (solid lines). The deposition and erosion of Upper Jurassic strata are omitted in scenario 2 as opposed to scenario 1. The maximum temperatures (dashed lines) attained during burial differ strongly, reflecting significant differences in heat flow. Neog. = Neogene; P. = Permian; Q. = Quaternary.

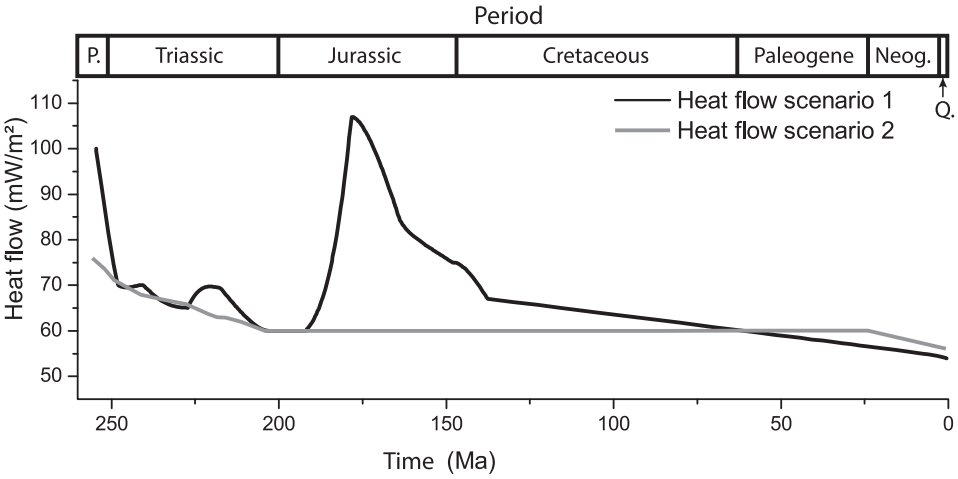

Figure 4. Comparison of heat flow scenarios for well B. Heat flow scenario 1 incorporates a peak between 200 and 145 Ma associated with Jurassic rifting and North Sea doming and is responsible for the modeled temperature peak in scenario 1 (Peisker, 2013). This scenario also incorporates a period of Upper Jurassic deposition and subsequent erosion (burial scenario 1, Figure 3B). Heat flow scenario 2 from Uffmann and Littke (2011) assumes that the Jurassic stretching and doming event did not affect heat flow in the study region. Neog. = Neogene; P. = Permian; Q. = Quaternary.

are used to constrain the amount of reactants and products of diagenetic reactions and the compaction history. The proportion of grain coat coverage of quartz grains was measured for 50 grains per sample. In total, 50 thin sections and associated plug samples were used as a basis for this study. Grain size measurements were performed on the long axis of at least 100 grains per sample on a grid adjusted to the maximum observed grain size to gain area-weighted results. Trask sorting was calculated from these measurements.

The modeling suite Touchstone™, developed by Geocosm LLC, encompasses algorithms to model the kinetics of quartz cement and fibrous illite growth (Lander et al., 2008; Lander and Bonnell, 2010) as well as compaction and the occurrence of various other cement types. Analog data from core material are used for this diagenetic forward modeling approach for reservoir quality modeling and prediction in sandstones. The kinetic parameters for each reaction are based on geologic constraints instead of experimental data. In the case of quartz cementation the primary kinetic parameter of interest is an activation energy (E_A) for crystal growth including changes in crystal growth rate depending on grain size and crystal domain size (Lander et al., 2008). The adjustable kinetic parameter for the fibrous illite model is an activation energy for the reaction of kaolinite and a potassium source (K-feldspar in this study) to form illite (Lander and Bonnell, 2010).

Additional model parameters constrain physical properties of detrital and authigenic phases related to their compaction behavior, as well as porosity and permeability. Compaction and the intergranular volume are modeled by using a proprietary algorithm (Makowitz et al., 2006; Lander et al., 2008) that builds on the concepts of Lander and Walderhaug (1999). The timing of the formation of authigenic phases in the paragenetic sequence can be constrained by thermal, temporal, or burial parameters and affects the compaction behavior and the development of the IGV over time. The IGV is typically measured by point counting from petrographic thin sections and is the sum of intergranular porosity, cements, and depositional matrix (Houseknecht, 1987; Paxton et al., 2002). The IGV simulation results reflect volumes and rigidities of authigenic and detrital mineral phases and effective stress through time (Lander and Walderhaug, 1999).

Additionally, the kinetic model of the alteration of kaolinite and feldspars to illite (Lander and Bonnell, 2010) has been used for simulations with Touchstone. Measured K-Ar ages of authigenic illite are used to evaluate the modeled time of formation as given by the diagenetic model (Zwingmann et al., 1999). The global error for K-Ar determinations was evaluated to be less than 2% (Zwingmann et al., 1999). Data of four size fractions (<0.2, 0.2–0.6, 0.6–1, and 1–2 μm) were analyzed and yielded ages from approximately 190 to 155 Ma (Zwingmann et al., 1998, 1999). Only samples from eolian deposits were chosen to avoid a contamination with detrital muscovite (Zwingmann et al., 1999). A deviation of the modeled illite ages from measured data would require an improved thermal reconstruction of the subsidence model or an adjustment of diagenetic

model parameters. The measured illite ages have not been used as an internal calibration within Touchstone.

Parameter optimization simulations have been carried out with respect to the activation energies described above as well as for compaction characteristics for the rock's solid components. This process is performed by iteratively changing parameters using a genetic algorithm and using a fitness function of the mean square difference between measured and simulated quartz cement volumes, illite cement volumes, and the IGV (Lander et al., 2008). The optimization simulation produces a parameter suite that yields an optimal match with measured values.

We used the quality of the optimization results as a means to evaluate the geological veracity of the two heat flow scenarios (Figures 3, 4). The heat flow scenarios were used to create two sets of 1-D burial models for each of the five wells. The paleosurface temperatures in both scenarios are based on reconstructions by Wygrala (1989) and are calculated by PetroMod™ depending on the present-day latitude. The lithotypes as defined by Peisker (2013) were not modified. The paleobathymetry is derived from facies maps from Ziegler (1990) and estimated from well logs (Peisker, 2013). The performance of both burial models with the same kinetic parameters for vitrinite maturation (EASY%R_o; Burnham and Sweeney, 1989) is comparable (Figure 3), although the thermal exposure in scenario 1 is much higher (Figure 4). The thermal exposure encompasses the time exposed to temperatures above which significant quartz cementation occurs.

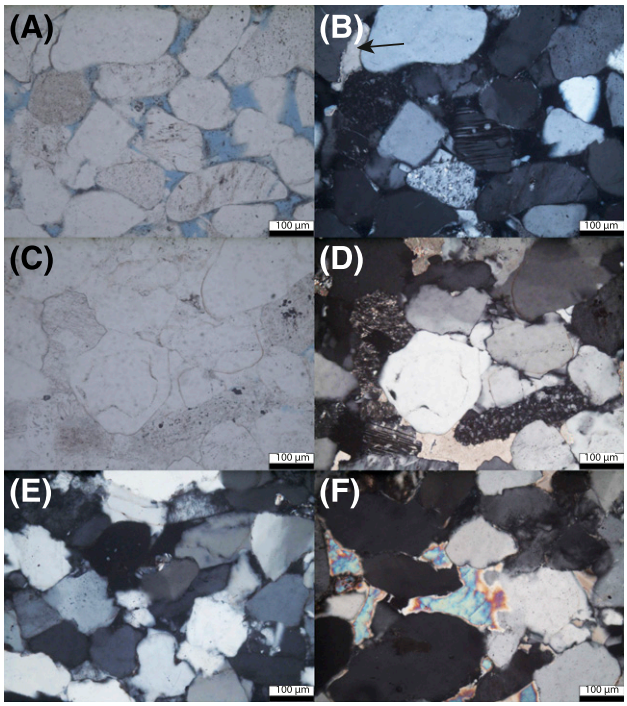

Figure 5. Photomicrographs of some representative Rotliegendes samples of dry sand flat deposits from the studied wells illustrate the different reservoir cementation types. Subsalt sample containing quartz and feldspar grains in (A) plane-polarized light (ppl) and (B) cross-polarized light (xpl). Significant intergranular porosity is retained by the presence of thin, faint greenish chlorite–smectite coatings, with white birefringence (well C). The coating phase, however, does not inhibit the growth of carbonate cement phases (arrow, top left). (C) A ppl image and (D) an xpl image. Large volumes of quartz cement occur in samples with poorly developed hematite or illite coatings (well E). (E) Pervasive quartz cementation also occurs in the absence of grain coating phases (ppl image, well B). (F) Authigenic cement phases such as anhydrite and carbonates occlude parts of the pore space in samples from every well (xpl image, well C).

RESULTS

Petrography

The sandstone samples (n = 50) contain between 48% and 69% detrital quartz grains including polycrystalline quartz grains, approximately 3%–15% feldspar grains (including plagioclase), and up to approximately 8% rock fragments (Figure 5, Table 1). Authigenic phases varying in content in different samples comprise approximately 2%–23% quartz cement, up to approximately 3% K-feldspar cement, up to 14% illite, up to 9% chlorite, up to 16% calcite cement (Figure 5B, D), and up to 20% sulfate cements including anhydrite (Figure 5F), gypsum, and barite (Table 1). Grain coating materials only present a small volumetric fraction of the samples (mean of 0.3%) and the main coating phases are chlorite and smectite–chlorite mixtures. The surface area of grains coated by either clay or hematite ranges from 5% to 97%. Samples with high grain coat coverages show substantially lower quartz cement abundances (Figure 5A, B), compared with samples with poorly developed coatings (Figure 5C–E). No apparent correlation exists between depositional environments and detrital composition, authigenic minerals, or grain coating coverage. The IGV of the sample set ranges from 16% to 39%. Higher values are associated with

Table 1. Data for 50 Samples Including the Depositional Environments, Modal Volumes, Intergranular Volumes, Coat Coverages, Grain Sizes and Sorting, and Petrophysical Data Measured on Associated Plug Samples

Sample ID	Well	Depositional Environment	Quartz	K-Feldspar	Plagioclase	Rock Fragments	Accessories	Iron Oxides	Matrix	Quartz Cement	Feldspar Cement	Carbonate Cement
A1	A	Dry sand flat	55.3	11.3	0.7	3.0	0.0	0.0	3.0	11.0	1.3	6.0
A2	A	Dune	61.7	9.7	0.3	1.7	0.0	0.3	5.0	3.7	0.0	1.3
A3	A	Damp sand flat	53.0	10.3	0.7	3.3	0.0	0.0	2.7	19.3	1.7	1.0
A4	A	Dry sand flat	56.3	11.3	0.3	1.7	0.0	0.0	1.7	9.0	2.7	2.0
A5	A	Dry sand flat	60.7	7.3	1.3	1.0	0.3	0.3	1.7	6.7	1.0	9.7
A6	A	Dry sand flat	60.7	8.7	0.3	4.7	0.3	0.0	1.7	5.0	1.0	3.7
A7	A	Dry sand flat	63.0	12.0	0.3	2.0	0.0	0.0	1.3	4.0	1.0	4.7
A8	A	Dry sand flat	61.3	6.3	0.7	2.7	0.3	0.0	1.0	9.3	1.0	9.3
A9	A	Dry sand flat	69.3	8.7	1.0	0.7	0.0	0.0	0.7	1.7	0.7	1.0
B1	B	Dune	51.0	7.7	2.0	5.7	0.3	1.3	2.3	12.7	0.7	7.0
B2	B	Dry sand flat	64.0	4.0	0.3	1.7	0.0	0.3	2.0	10.7	1.3	11.7
B3	B	Dune	55.3	5.0	1.0	1.3	0.0	1.3	1.3	13.3	1.0	10.3
B4	B	Dune	56.0	4.0	2.3	1.0	0.0	1.0	1.7	13.7	1.0	10.3
B5	B	Dry sand flat	57.3	6.7	2.3	3.3	0.0	1.0	1.3	11.7	0.7	7.7
B6	B	Dry sand flat	53.7	7.0	1.0	5.7	0.7	0.3	1.7	13.0	0.7	1.7
B7	B	Dry sand flat	63.3	5.0	1.3	2.7	0.0	0.3	0.7	7.7	2.7	0.3
B8	B	Dry sand flat	67.7	4.0	2.0	3.7	0.3	0.0	0.3	12.0	1.3	0.7
B9	B	Damp sand flat	60.0	3.3	1.0	2.7	1.0	0.7	5.7	5.0	0.3	1.0
B10	B	Dry sand flat	61.7	5.7	0.7	5.7	0.0	0.7	1.7	12.3	2.3	4.7
C1	C	Dune	65.3	6.7	1.3	5.7	0.7	0.0	1.3	4.0	0.3	3.0
C2	C	Dry sand flat	67.3	5.7	1.0	3.7	0.0	0.0	1.0	8.7	0.0	7.7
C3	C	Dry sand flat	64.0	6.7	1.3	2.0	0.0	0.0	0.0	11.0	0.0	5.0
C4	C	Dune	56.3	6.7	2.0	7.7	0.0	0.3	0.3	6.3	1.7	4.0
C5	C	Dune	62.3	9.0	0.7	2.0	0.3	0.0	1.0	5.0	1.3	2.3
C6	C	Dune	54.7	8.0	2.0	4.0	0.0	0.0	0.3	8.3	1.0	1.7
C7	C	Dry sand flat	58.3	10.7	1.3	4.7	0.0	0.0	0.7	5.7	0.7	2.3
C8	C	Damp sand flat	59.0	6.3	0.3	3.7	0.3	0.0	0.0	4.0	0.7	1.7
D1	D	Dune	60.0	10.3	0.0	2.3	1.3	0.3	0.3	11.3	1.3	4.0
D2	D	Dune	49.0	10.0	1.3	4.0	0.7	0.3	0.3	12.7	0.3	8.0
D3	D	Dune	58.0	10.3	0.7	1.7	0.3	0.0	0.3	9.7	1.7	2.7
D4	D	Dry sand flat	61.7	8.3	0.7	1.0	0.0	0.3	0.0	17.7	1.0	6.0
D5	D	Dry sand flat	58.0	8.7	0.3	3.3	0.3	0.3	0.3	7.3	0.7	16.3
D6	D	Damp sand flat	59.0	11.0	1.3	1.0	0.7	2.7	0.7	16.3	0.7	1.3
D7	D	Dry sand flat	56.7	10.0	0.0	5.0	0.0	3.7	0.0	18.3	0.3	1.7
D8	D	Dry sand flat	57.7	14.0	1.0	2.0	0.0	1.0	0.3	7.7	0.3	11.7
D9	D	Dry sand flat	50.7	9.0	0.3	1.7	0.3	0.7	0.3	11.3	2.0	9.0
D10	D	Dry sand flat	55.7	7.0	0.7	1.7	0.0	0.3	0.7	6.7	0.0	6.3
E1	E	Lake margin	48.0	7.7	1.3	2.0	0.3	0.3	2.0	8.0	0.3	12.0
E2	E	Dry sand flat	63.0	7.3	1.3	3.7	0.0	0.0	0.0	9.0	2.0	3.7
E3	E	Dry sand flat	64.3	6.0	1.0	1.3	0.0	0.0	1.0	12.0	2.3	8.3
E4	E	Dry sand flat	63.7	9.3	1.7	3.0	0.0	0.0	1.0	5.7	1.3	1.0
E5	E	Dry sand flat	62.0	8.3	2.0	2.0	0.7	0.0	0.3	5.3	1.0	6.7
E6	E	Dry sand flat	57.3	7.0	1.0	1.0	0.3	0.0	1.0	22.7	1.7	4.3
E7	E	Dry sand flat	55.7	6.0	1.7	1.0	0.3	0.3	0.7	9.3	2.0	10.0
E8	E	Dry sand flat	54.7	4.3	0.7	1.7	0.0	0.0	0.0	8.0	2.0	13.3
E9	E	Dry sand flat	59.7	6.7	1.0	1.3	0.3	0.0	1.0	3.7	1.0	13.7
E10	E	Dry sand flat	57.3	11.0	1.0	1.7	0.0	0.0	0.7	3.7	1.0	1.3
E11	E	Dry sand flat	58.0	7.0	0.7	3.7	0.0	0.0	0.7	10.0	0.7	3.3
E12	E	Dry sand flat	61.0	11.7	0.7	0.0	0.3	0.0	0.0	5.7	0.7	14.7
E13	E	Dry sand flat	53.7	6.0	0.3	2.3	0.0	0.0	0.7	11.3	0.3	9.7

Abbreviation: ms = moderately sorted.

Table 1. Continued

Sulfate Cement	Illite Cement	Illite Replacement	Chlorite Cement	Chlorite Replacement	Intergranular Porosity	Secondary Porosity	Intergranular Volume (%)	Coat Coverage (%)	Mean Grain Size (mm)	Sorting	Plug Porosity (%)	Plug Permeability (md)
0.0	0.0	2.0	0.0	0.0	5.3	1.0	23.7	70.5	0.212	ms	8.2	8.70
12.0	0.0	2.3	1.7	0.3	0.0	0.0	18.7	80.5	0.186	ms	2.0	0.07
0.3	0.0	2.7	0.3	0.0	2.7	2.0	25.3	79.9	0.186	ms	6.7	1.06
0.3	0.0	1.0	2.7	0.0	9.7	1.3	26.3	88.8	0.167	ms	12.8	43.50
1.7	0.7	2.0	3.7	0.0	1.7	0.3	25.0	86.2	0.181	ms	5.9	0.17
0.0	0.0	1.7	4.7	0.0	7.0	0.7	21.3	92.7	0.240	ms	11.8	43.50
1.0	0.0	2.7	4.0	0.0	3.7	0.3	18.3	87.2	0.164	ms	8.7	4.20
1.0	0.0	2.0	2.7	0.3	1.3	0.7	24.7	68.1	0.166	ms	5.2	0.10
0.3	0.0	1.7	6.0	0.0	7.0	1.3	16.7	97.2	0.248	ms	20.6	n.a.
7.7	0.0	1.0	0.0	0.0	0.7	0.0	28.7	48.5	0.221	ms	2.1	0.06
3.0	0.0	1.0	0.0	0.0	0.0	0.0	26.7	35.1	0.197	ms	1.7	0.03
9.7	0.0	0.3	0.0	0.0	0.0	0.0	34.3	20.2	0.147	ms	2.3	0.04
8.0	0.0	0.3	0.0	0.0	0.3	0.3	33.3	13.8	0.155	ms	2.3	0.05
2.3	0.0	0.7	0.0	0.3	4.3	0.3	26.7	9.3	0.164	ms	8.6	0.66
4.0	0.0	1.0	0.0	0.0	9.0	0.0	28.3	13.7	0.200	ms	10.8	11.70
5.3	0.0	1.0	0.0	0.0	9.3	0.3	25.3	11.8	0.175	ms	11.1	26.50
1.7	0.0	1.3	0.0	0.0	4.0	0.0	19.7	10.6	0.167	ms	10.3	11.10
14.7	3.7	1.0	0.0	0.0	0.0	0.0	24.6	22.9	0.143	ms	2.0	0.02
2.3	0.3	0.3	0.0	0.0	1.7	0.0	23.7	18.6	0.184	ms	5.2	0.09
0.3	1.0	2.3	6.3	0.0	0.7	1.0	15.7	92.4	0.183	ms	4.5	0.04
2.3	0.3	1.0	0.3	0.3	0.3	0.3	19.7	83.4	0.180	ms	3.5	0.04
1.0	2.3	1.3	3.3	0.0	1.7	0.0	24.3	85.4	0.177	ms	4.2	0.03
4.3	0.0	1.0	4.3	0.3	4.0	0.3	24.7	97.3	0.248	ms	5.8	0.09
5.7	0.3	2.0	2.3	0.3	5.0	0.3	22.0	89.4	0.172	ms	8.9	1.46
12.3	0.3	0.7	2.3	1.0	2.7	0.7	28.7	79.1	0.187	ms	5.9	0.25
5.3	0.0	0.7	4.7	0.0	0.7	0.3	19.3	89.4	0.188	ms	8.2	2.63
0.0	13.0	1.0	7.7	1.0	0.0	1.7	27.0	87.8	0.174	ms	0.9	0.01
5.7	0.3	0.3	0.0	0.0	2.3	0.0	25.0	32.4	0.216	ms	4.7	0.34
7.0	0.0	1.3	0.0	0.3	4.0	0.7	32.0	41.2	0.218	ms	6.4	2.37
6.7	0.0	1.0	0.0	0.3	4.3	2.3	25.0	42.9	0.229	ms	8.0	13.40
1.0	0.0	1.3	0.0	0.0	0.3	0.7	26.0	8.8	0.226	ms	4.3	0.23
2.7	0.0	0.7	0.0	0.7	0.0	0.3	27.0	5.4	0.313	ms	3.8	0.07
2.0	0.0	0.7	0.0	0.0	2.0	0.7	22.3	68.8	0.199	ms	6.5	0.29
0.7	0.0	0.7	0.0	0.7	0.3	1.7	21.3	28.6	0.290	ms	6.1	0.15
2.7	0.0	1.0	0.0	0.3	0.0	0.3	22.3	13.3	0.285	ms	3.0	0.06
14.7	0.0	0.0	0.0	0.0	0.0	0.0	37.0	19.9	0.203	ms	1.9	n.a.
20.0	0.0	0.7	0.0	0.3	0.0	0.0	33.0	15.3	0.216	ms	1.1	0.03
17.0	0.0	1.0	0.0	0.0	0.0	0.0	37.3	65.1	0.177	ms	0.9	35.00
1.7	0.0	0.0	0.0	0.0	7.0	1.3	23.3	30.2	0.200	ms	9.3	5.10
1.3	0.0	0.7	0.0	0.3	0.7	0.3	24.7	66.2	0.186	ms	n.a.	n.a.
1.3	0.0	0.3	0.0	0.3	9.3	2.0	18.7	81.3	0.168	ms	11.7	22.30
1.0	0.3	0.0	0.0	0.3	8.3	1.7	22.7	84.9	0.155	ms	13.9	41.80
0.0	0.0	0.7	0.0	0.0	2.3	0.7	31.0	70.5	0.162	ms	5.8	0.13
3.7	0.7	1.0	0.0	0.0	7.3	0.3	33.0	90.3	0.160	ms	6.9	0.53
15.3	0.0	0.0	0.0	0.0	0.0	0.0	38.7	8.3	0.178	ms	1.8	0.05
2.0	3.0	2.7	0.0	0.0	4.0	0.0	27.3	41.2	0.187	ms	5.3	0.26
4.7	0.0	1.7	0.0	0.3	12.7	1.0	23.3	91.3	0.178	ms	15.9	122.00
2.0	1.0	1.0	1.3	0.0	8.7	1.3	27.0	87.5	0.179	ms	10.6	15.00
3.0	0.3	0.7	0.0	0.3	0.0	1.0	24.3	48.6	0.164	ms	4.2	0.05
11.0	1.0	1.3	0.0	0.0	1.3	1.0	34.7	34.6	0.168	ms	2.8	0.08

early carbonate and sulfate cements. The petrophysically derived porosity ranges from 0.9% to 20.6%, and permeability ranges from 0.01 to 122 md. The petrophysical measurements of associated plug samples are given in Table 1.

Quartz Kinetics Calibration

The Touchstone model-generated volumes of quartz cement derived using thermal histories from the two thermal models are compared with the volume of quartz cement present in the samples as determined by petrographic point count analyses. The results are then used as a test of the veracity of the two fundamentally different thermal models. The quartz cementation kinetic parameters include an activation energy (E_A) for crystal growth along the c axis on noneuhedral surfaces and a pre-exponential parameter (A_O) (Lander et al., 2008). This growth model is based on the Prism2D algorithm for surface area normalized crystal growth (Lander et al., 2008; Lander and Laubach, 2014). During parameter optimization we allowed the E_A value to range between 55 and 65 kJ/mol and fixed the A_O value at 9×10^{12} mol/cm^2/s. These values are consistent with ranges reported by Lander et al. (2008) for quartz cementation in sandstones from four geologically diverse data sets. All samples within a given scenario are subject to the same set of kinetic parameters.

We obtained an optimized E_A value of 58.2 kJ/mol in the higher-temperature heat flow model (scenario 1). The calculated quartz cement values deviate from measured values by a maximum of 12 vol. %. The quartz cement values tend to be overpredicted for wells B, D, and E but underpredicted for subsalt well C (Figure 6A). The only good fit for this model scenario is for samples from well A. To create a reasonable fit of measured versus calculated data for the other wells, we conducted parameter optimization for each well individually, disregarding samples from other wells. The quartz activation energies obtained by this method ranged from values exceeding 65 kJ/mol for wells B and D, to less than 55 kJ/mol for well C. We deem this thermal scenario to be inconsistent with the quartz cement abundances in these wells because of the combination of (1) poor model performance for the case where the same kinetic parameters are used for all wells, (2) optimized E_A values derived from individual wells that are widely divergent despite close proximities, and (3) E_A values from individual wells that are outside of the ranges reported elsewhere (i.e., Makowitz et al., 2006; Lander et al., 2008).

By contrast, the lower-temperature scenario 2 results in modeled quartz cement values that closely correspond to measured values from thin section analysis (Figure 6B). The derived E_A for quartz cementation of 58.2 kJ/mol is used for samples from all wells and is well within the range of values reported from other data sets. The quartz cement volumes are

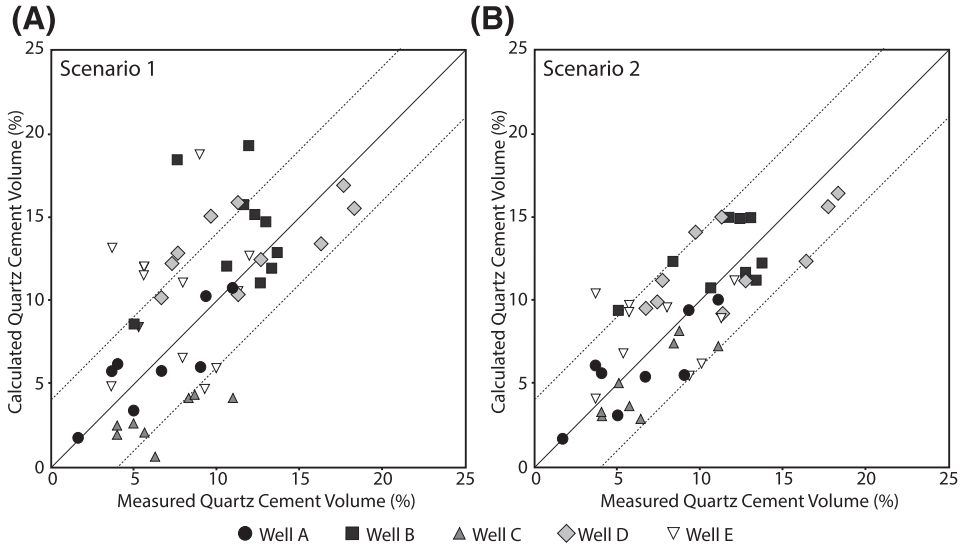

Figure 6. Comparison of the performance of the quartz cement model for the two thermal history scenarios. (A) The high-temperature scenario 1 results in a systematic overprediction of quartz cements for wells B, D, and E. The deviation from measured amounts of quartz cement is up to 12%, well outside of the likely measurement uncertainty of approximately 4% (dotted lines). However, simulations using scenario 1 for subsalt samples from well C underpredict the amount of measured quartz cement by up to 7%. (B) Modeled quartz cement values match data from all study wells within the likely measurement uncertainty for most samples of ±4%.

well reproduced in samples from all represented depositional environments.

Illite Kinetics Calibration

As an additional evaluation of the two alternative thermal scenarios we also evaluate the performance of a kinetic model for illite formation. In this case we use the kinetic constraints from Lander and Bonnell (2010).

For the high-temperature scenario 1 the formation of illite is predicted to be in a range between 245 and 195 Ma (Figure 7A), which predates the measured values (Figure 7B) of Zwingmann et al. (1998). By contrast, the start of illite formation in scenario 2 (Figure 7C) is modeled to be at 210 Ma and to have ceased at 155 Ma, which is consistent with measured K-Ar ages of illite (Platt, 1993; Zwingmann et al., 1999) in the North German Basin on the Pompeckj Block. Peak formation rates match the measured K-Ar ages of illite in a nearby Rotliegendes graben of 190–155 Ma (Figure 7B) (Zwingmann et al., 1998). The maximum illite formation rate in scenario 1 is nearly twice as high as in scenario 2 (Figure 7A,

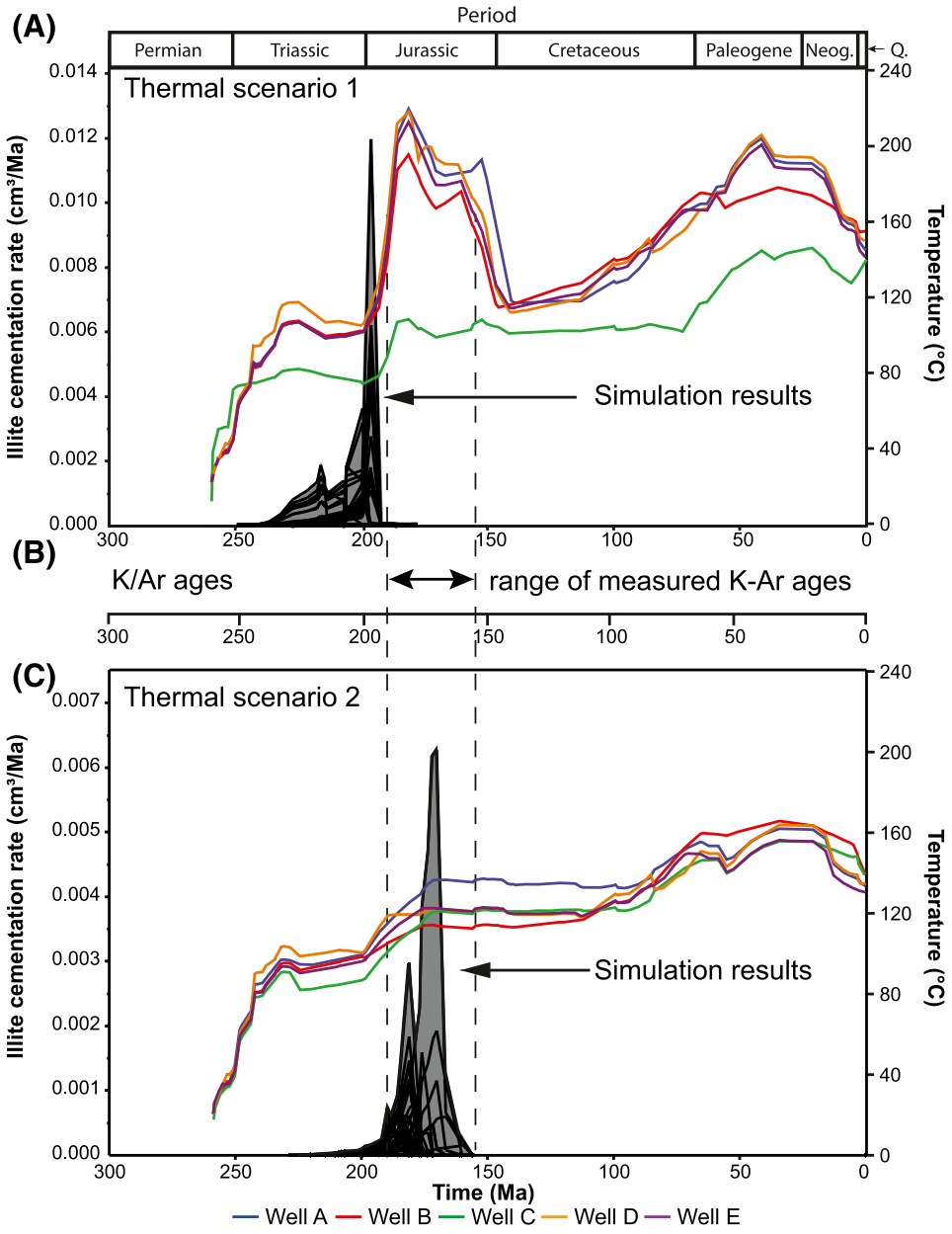

Figure 7. (A) Comparison of modeled rate of illite formation (black line) for thermal scenario 1 of wells A–E (dashed lines). The black filled region marked as "simulation results" shows the modeled volumetric rate of illite formation through time. Note that the results for this scenario show illite formation beginning prior to the oldest K-Ar date. (B) The K-Ar ages of illites from the Rotliegende in the North German Basin from Zwingmann et al. (1998, 1999). (C) The illite simulation results for burial scenario 2 predicts peak illite formation for each well to be within the range of measured illite ages. The thermal reconstructions for wells A–E are given as the colored lines. Neog. = Neogene; Q. = Quaternary.

C). However, this rate difference is restricted to few samples with larger measured illite contents. Simulated illite cement volumes match measured data equally well for both scenarios given that in both cases, kaolinite reactants have been fully consumed in the geologic past (Figure 8).

Porosity, Permeability, and Intergranular Volume

Given that thermal scenario 2 is far more consistent with observed quartz and illite cement volumes and characteristics, we used this scenario as a basis for developing a general reservoir quality prediction model. This model provides very good performance for total porosity, permeability, and intergranular volume (Figure 9). The calculated porosities are within 4 vol. % of the measured values that range from 1 to 16 vol. % (Figure 9A), apart from one porosity measurement from well A. The permeability values, which range from 0.1 to 100 md (Figure 9B), are similarly well matched with only two lower permeability predictions being in error by more than a factor of 10. The measured IGV values, which range from 16% to 37%, are generally matched within 4 vol. % by the simulations (Figure 9C).

DISCUSSION AND CONCLUSIONS

Although thermal scenario 1 provides an acceptable match to measured present-day bottomhole temperature and vitrinite reflectance data, it leads to overprediction of quartz cement abundance for wells B, D, and E and underprediction of quartz cement from well C when a single set of kinetic parameters is used for samples from all wells. These results suggest that the scenario 1 thermal exposure is greater than indicated by quartz cement abundances for scenario 1 for wells A, B, D, and E and lower for well C. Additionally, this thermal scenario leads to predicted timing of illite formation that predates K-Ar dates of illite from the region. Considering the uncertainty in ages (given as $\pm 2\sigma$ of the age determination), which is between 4 and 6 Ma, illite formation in scenario 1 is still too early (cf. Zwingmann et al., 1998, 1999).

In light of the poor match with quartz cement and illite data we adapted heat flow scenario 2 from heat flow reconstructions from Schwarzer and Littke (2007) and Uffmann and Littke (2011), which contrasts with scenario 1 in that the heat flow increase during the Jurassic is omitted. Typical continental heat flow values of approximately 55–60 mW/m^2 since the Jurassic sufficiently model the maturation of organic matter in this part of the North German Basin. The additional rifting phases in the North German Basin do not lead to an increase in heat flow in the basin models from which the heat flow was derived. Thermal histories from this scenario have an equivalent quality of fit to present-day temperature and vitrinite reflectance data as heat flow scenario 1 (Figure 3) while also providing far superior performance for reconstructing quartz cement abundances (Figure 6) and the timing of illite formation (Figure 7). The times of the peak rates of illite formation modeled in scenario 2 are consistent with the range in K-Ar dates from samples originating

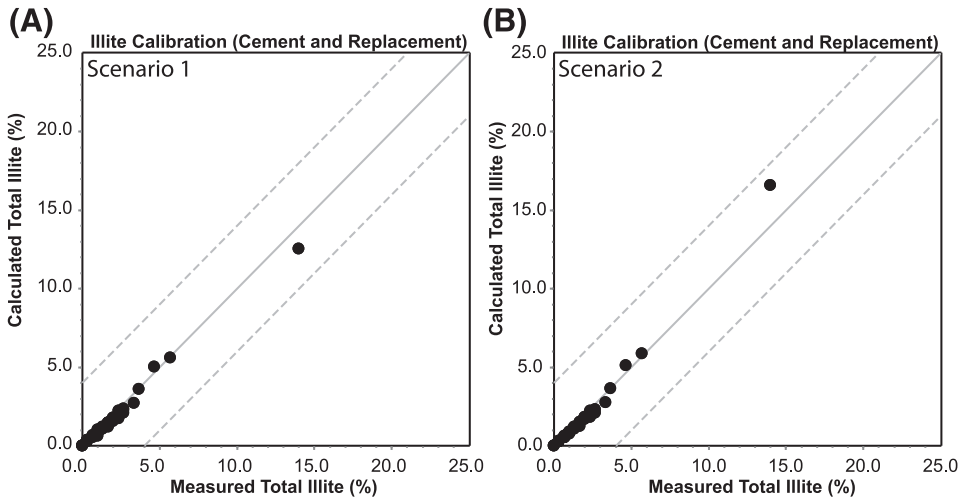

Figure 8. Comparison of the modeling results to reproduce measured amounts of illite cement. (A) Scenario 1 and (B) scenario 2 both reproduce point-counted illite volumes within 4%.

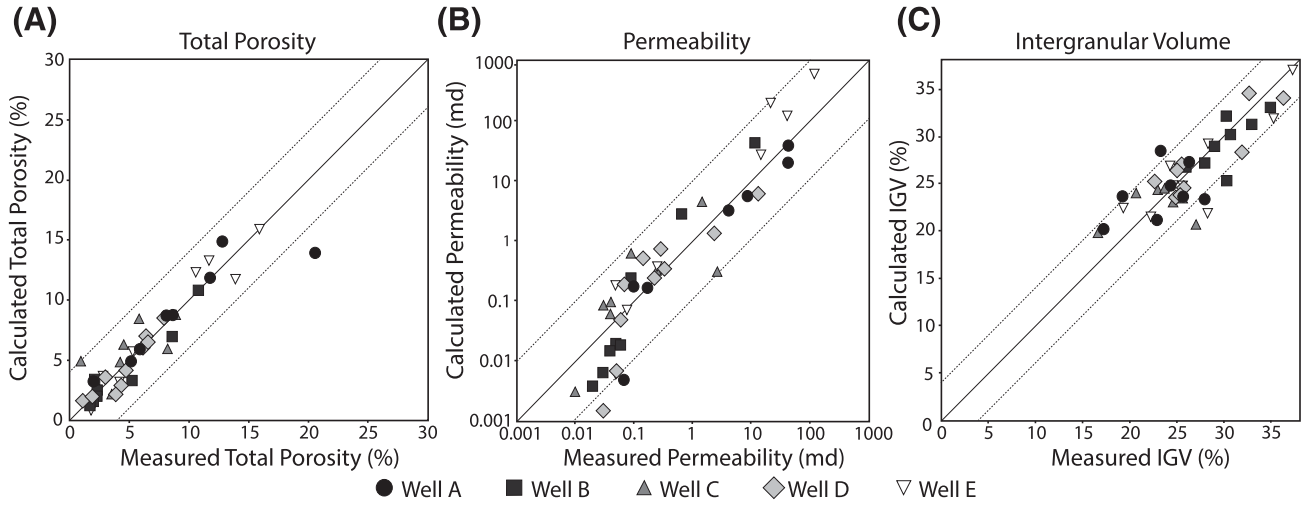

Figure 9. Calibration plots based on burial scenario 2 showing measured values on the *x* axis and the model predicted values for the present day on the *y* axis. (A) Total porosities. (B) Permeabilities. (C) Intergranular volumes (IGV).

from a Rotliegendes graben (190–155 Ma; Zwingmann et al., 1998)

Our results illustrate the utility of using diagenetic models for constraining thermal histories. Although quartz cementation rates are strongly affected by temperature, the overall abundance of quartz is far more sensitive to elapsed time compared with organic paleothermal indicators such as vitrinite reflectance (Awwiller and Summa, 1997; Lander et al., 1997a, b; Perez et al., 1999). Recent publications highlight the accuracy of both quartz cementation kinetic models (Harwood et al., 2013) and vitrinite reflectance kinetic models (Le Bayon et al., 2012).

The kinetic model for fibrous illite formation is comparable to that of quartz with respect to the effect of both time and temperature. However, although quartz overgrowth cementation is a process that appears to continue so long as nucleation surface area is available, the illitization reaction stops once the reactants are consumed (in this case, kaolinite was fully consumed, leaving residual K-feldspar). Consequently, this reaction has the potential to provide useful information about absolute time that may be tested by comparison with radiometric dates (Lander and Bonnell, 2010). In this study a simulation using the scenario 2 burial history model matched illite K-Ar dates that correspond to 190–155 Ma. It is notable that temperatures at this time were significantly below maximum values that were reached later in the thermal history.

The implications of improving constraints on thermal histories are of enormous importance not only in the study area but in many, if not most, hydrocarbon provinces. Thermal history is a primary control on the timing of hydrocarbon generation and oil-to-gas cracking, which in turn affects hydrocarbon migration and the likely fluid types in undrilled reservoirs. Thermal history also clearly is a direct control on diagenetic processes of fundamental importance for reservoir quality. Quartz cementation and fibrous illite crystal growth kinetics provide uniquely powerful means for constraining thermal reconstructions when used in concert with well-established organic paleothermometers and petroleum systems modeling methods.

REFERENCES CITED

Ajdukiewicz, J. M., and R. H. Lander, 2010, Sandstone res ervoir quality prediction: The state of the art: AAPG Bulletin, v. 94, no. 8, p. 1083 1091, doi:10.1306/intro060110.

Ajdukiewicz, J. M., and R. E. Larese, 2012, How clay grain coats inhibit quartz cement and preserve porosity in deeply buried sandstones: Observations and experiments: AAPG Bulletin, v. 96, no. 11, p. 2091 2119, doi:10 .1306/02211211075.

Allen, P. A., and J. R. Allen, 2005, Basin analysis Principles and applications: Malden, Masachusetts, Blackwell, 560 p.

Awwiller, D. N., and L. L. Summa, 1997, Quartz cement volume constraints on burial history analysis: An example from the Eocene of western Venezuela (abs.): AAPG Search and Discovery article 91021, accessed December 2, 2015, http: //www.searchanddiscovery.com/abstracts/html/1997 /annual/abstracts/0006c.htm.

Baldschuhn, R., F. Binot, S. Fleig, and F. Kockel, 2001, Geotektonischer Atlas von Nordwest Deutschland und dem deutschen Nordsee Sektor:Stuttgart, Germany, E. Schweizerbart'sche Verlagsbuchhandlung, Geologisches Jahrbuch 153, 88 p.

Bombien, H., B. Hoffers, S. Breuckmann, M. Helms, K. Lademann, M. Lange, A. Oelrich, et al., 2012, Der Geotektonische Atlas von Niedersachsen und dem deutschen Nordseesektor als geologisches 3D Modell: Bonn, Germany, Geowissenschaftliche Mitteilungen, p. 6 13.

Bruns, B., R. di Primio, U. Berner, and R. Littke, 2013, Petroleum system evolution in the inverted Lower Saxony Basin, northwest Germany: A 3D basin modeling study: Geofluids, v. 13, p. 246 271, doi:10.1111/gfl.12016.

Burnham, A. K., and J. J. Sweeney, 1989, A chemical kinetic model of vitrinite maturation and reflectance: Geochimica et Cosmochimica Acta, v. 53, p. 2649 2657, doi:10.1016/0016 7037(89)90136 1.

French, M. W., R. H. Worden, E. Mariani, R. E. Larese, R. R. Mueller, and C. E. Kliewer, 2012, Microcrystalline quartz generations and the preservation of porosity in sandstones: Evidence from the Upper Cretaceous of the Subhercynian Basin, Germany: Journal of Sedimentary Research, v. 82, p. 422 434, doi:10.2110/jsr.2012.39.

Gier, S., R. H. Worden, W. D. Johns, and H. Kurzweil, 2008, Diagenesis and reservoir quality of Miocene sandstones in the Vienna Basin, Austria: Marine and Petroleum Geology, v. 25, p. 681 695, doi:10.1016/j.marpetgeo.2008.06.001.

Harwood, J., A. C. Aplin, C. I. Fialips, J. Iliffe, R. Kozdon, T. Ushikubo, and J. W. Valley, 2013, Quartz cementation history of sandstone revealed by high resolution SIMS oxygen isotope analysis: Journal of Sedimentary Research, v. 83, p. 522 530, doi:10.2110/jsr.2013.29.

Heald, M. T., and R. E. Larese, 1974, Influence of coatings on quartz cementation: Journal of Sedimentary Petrology, v. 44, p. 1269 1274, doi:10.1306/212F6C94 2B24 11D7 8648000102C1865D.

Houseknecht, D. W., 1987, Assessing the relative importance of compaction processes and cementation to reduction of porosity in sandstones: AAPG Bulletin, v. 71, no. 6, p. 633 642.

Lander, R. H., and L. M. Bonnell, 2010, A model for fibrous illite nucleation and growth in sandstones: AAPG Bulletin, v. 94, no. 8, p. 1161 1187, doi:10.1306/04211009121.

Lander, R. H., V. Felt, L. M. Bonnell, and O. Walderhaug, 1997a, Utility of sandstone diagenetic modeling for basin history assessment (abs.): AAPG Search and Discovery article 91021, accessed December 2, 2015, http://www.searchanddiscovery.com/abstracts/html/1997/annual/abstracts/0066b.htm.

Lander, R. H., R. E. Larese, and L. M. Bonnell, 2008, Toward more accurate quartz cement models: The importance of euhedral versus noneuhedral growth rates: AAPG Bulletin, v. 92, no. 11, p. 1537 1563, doi:10.1306/07160808037.

Lander, R. H., and S. E. Laubach, 2014, Insights into rates of fracture growth and sealing from a model for quartz cementation in fractured sandstones: Geological Society of America Bulletin, v. 127, p. 516 538, doi:10.1130/B31092.1.

Lander, R. H., and O. Walderhaug, 1999, Predicting porosity through simulating sandstone compaction and quartz cementation: AAPG Bulletin, v. 83, no. 3, p. 433 449, doi:10.1306/00AA9BC4 1730 11D7 8645000102C1865D.

Lander, R. H., O. Walderhaug, and L. M. Bonnell, 1997b, Application of sandstone diagenetic modeling to reservoir quality prediction and basin history assessment, *in* Memorias del I Congreso Latinoamericano de Sedimentología: Caracas, Venezuela, Sociedad Venezolana de Geólogos, November 16 19, 1997, p. 373 386.

Le Bayon, R., S. Buhre, B. C. Schmidt, and R. F. Mählmann, 2012, Experimental organic matter maturation at 2kbar: Heat up effect to low temperatures on vitrinite reflectance: International Journal of Coal Geology, v. 92, p. 45 53, doi:10.1016/j.coal.2011.12.002.

Littke, R., M. Scheck Wenderoth, M. R. Brix, and S. Nelskamp, 2008, Subsidence, inversion and evolution of the thermal field, *in* R. Littke, U. Bayer, D. Gajewski, and S. Nelskamp, eds., Dynamics of complex intracontinental basins The Central European basin system: Berlin, Springer, p. 125 153, doi:10.1007/978 3 540 85085 4.

Makowitz, A., R. H. Lander, and K. L. Milliken, 2006, Diagenetic modeling to assess the relative timing of quartz cementation and brittle grain processes during compaction: AAPG Bulletin, v. 90, no. 6, p. 873 885, doi:10.1306/12190505044.

Matthews, J. M., J. Samuelson, C. Lowrey, and H. M. Helset, 2002, Quartz cement abundance as a thermal history indicator A case study from the Gjallar Ridge, Vøring Basin (abs.): AAPG Search and Discovery article 90022, accessed December 2, 2015, http://www.searchanddiscovery.com/pdfz/abstracts/pdf/2002/hedberg norway/extended/ndx matthews.pdf.html.

McKenzie, D., 1978, Some remarks on the development of sedimentary basins: Earth and Planetary Science Letters, v. 40, p. 25 32, doi:10.1016/0012 821X(78)90071 7.

Meng, Y., C. Xu, H. Xie, W. Tian, C. Tong, J. Liu, Y. Wang, and Y. Gao, 2013, A new kinetic model for authigenic quartz formation under overpressure: Petroleum Exploration and Development, v. 40, p. 751 757, doi:10.1016/S1876 3804(13)60100 7.

Menning, M., 1995, A numerical time scale for the Permian and Triassic periods: An integrated time analysis, *in* P. A. Scholle, T. M. Peryt, and D. S. Ulmer Scholle, eds., Paleogeography, paleoclimates, stratigraphy, Berlin, Springer, The Permian of Northern Pangea 1, p. 77 97.

Oelkers, E. H., P. Bjørkum, and W. M. Murphy, 1996, A petrographic and computational investigation of quartz cementation and porosity reduction in North Sea sandstones: American Journal of Science, v. 296, p. 420 452, doi:10.2475/ajs.296.4.420.

Paxton, S. T., J. O. Szabo, J. M. Ajdukiewicz, and R. E. Klimentidis, 2002, Construction of an intergranular compaction curve for evaluating and predicting compaction and porosity loss in rigid grain sandstone reservoirs: AAPG Bulletin, v. 86, no. 12, p. 2047 2067.

Peisker, J., 2013, Vorhersagbarkeit der reservoireigenschaften in Rotliegend Sandsteinen des Gebietes Dreilingen NE Hannover, Deutschland, Diplom thesis, Friedrich Schiller Universität Jena, Jena, Germany, 109 p.

Perez, R. J., J. I. Chatellier, and R. H. Lander, 1999, Use of quartz cementation kinetic modeling to constrain burial histories. Examples from the Maracaibo Basin, Venezuela: Revista Latino Americana de Geoquimica Organica, v. 5, p. 39 46.

Pharaoh, T. C., M. Dusar, M. C. Geluk, F. Kockel, C. Krawczyk, P. Krzywiec, M. Scheck Wenderoth, H. Thybo, O. V. Vejbæk, and J. D. Van Wees, 2010, Tectonic evolution, *in* H. Doornenbal and A. Stevenson, eds., Petroleum geological atlas of the southern Permian Basin area: Houten, Netherlands, European Association of Geoscientists and Engineers, p. 25 57.

Platt, J. D., 1993, Controls on clay mineral distribution and chemistry in the early Permian Rotliegend of Germany: Clay Minerals, v. 28, p. 393 416, doi:10.1180/claymin.1993.028.3.05.

Rimstidt, J. D., and H. L. Barnes, 1980, The kinetics of silica water reactions: Geochimica et Cosmochimica Acta, v. 62, p. 1851 1863, doi:10.1016/S0016 7037(98)00125 2.

Schöner, R., 2006, Comparison of Rotliegend sandstone diagenesis from the northern and southern margin of the North German Basin, and implications for the importance of organic maturation and migration, Ph.D. thesis, Friedrich Schiller Universität Jena, Jena, Germany, 230 p.

Schöner, R., and R. Gaupp, 2005, Contrasting red bed diagenesis: The southern and northern margin of the Central European Basin: International Journal of Earth Sciences, v. 94, p. 897 916, doi:10.1007/s00531 005 0004 3.

Schwarzer, D., and R. Littke, 2007, Petroleum generation and migration in the 'Tight Gas' area of the German Rotliegend natural gas play: A basin modeling study: Petroleum Geoscience, v. 13, p. 37 62, doi:10.1144/1354 079306 703.

Sindern, S., H. Stanjek, C. Hilgers, and Y. Etoundi, 2007, Short term hydrothermal effects on the 'crystallinities' of illite and chlorite in the footwall of the Aachen Faille du midi thrust fault First results of the RWTH 1 drilling project: Clays and Clay Minerals, v. 55, p. 200 212, doi:10.1346/CCMN.2007.0550209.

Taylor, T. R., M. R. Giles, L. A. Hathon, T. N. Diggs, N. R. Braunsdorf, G. V. Birbiglia, M. G. Kittridge, C. I. Macaulay, and I. S. Espejo, 2010, Sandstone diagenesis and reservoir quality prediction: Models, myths, and reality: AAPG Bulletin, v. 94, no. 8, p. 1093 1132, doi:10.1306/04211009123.

Taylor, T. R., M. G. Kittridge, P. Winefield, L. T. Bryndzia, and L. M. Bonnell, 2015, Reservoir quality and rock properties modeling Triassic and Jurassic sandstones, greater Shearwater area, UK Central North Sea: Marine and Petroleum Geology, v. 65, p. 1 21, doi:10.1016/j.marpetgeo.2015.03.020.

Taylor, T., R. Stancliffe, C. Macaulay, and L. Hathon, 2004, High temperature quartz cementation and the timing of hydrocarbon accumulation in the Jurassic Norphlet sandstone, offshore Gulf of Mexico, USA, *in* J. M. Cubitt, W. A. England, and S. Larter, eds., Understanding petroleum reservoirs: Towards an integrated reservoir engineering and geochemical approach: Geological Society, London, Special Publications 2004, v. 237, p. 257 278, doi:10.1144/GSL.SP.2004.237.01.15.

Uffmann, A. K., and R. Littke, 2011, 3D petroleum systems modelling of the North German Basin: First Break, v. 29, p. 49 63, doi:10.3997/1365 2397.2011016.

Walderhaug, O., 1994, Precipitation rates for quartz cement in sandstones determined by fluid inclusion microthermometry and temperature history modeling: Journal of Sedimentary Research, v. A64, p. 324 333, doi:10.2110/jsr.64.324.

Walderhaug, O., 1996, Kinetic modelling of quartz cementation and porosity loss in deeply buried sandstone reservoirs: AAPG Bulletin, v. 80, no. 5, p. 731 745, doi:10.1306/64ED88A4 1724 11D7 8645000102C1865D.

Walderhaug, O., 2000, Modeling quartz cementation and porosity in middle Jurassic Brent Group sandstones of the Kvitebjorn Field, Northern North Sea: AAPG Bulletin, v. 84, no. 9, p. 1325 1339, doi:10.1306/A9673E96 1738 11D7 8645000102C1865D.

Walderhaug, O., R. H. Lander, P. A. Bjørkum, H. Oelkers, K. Bjørlykke, and P. H. Nadeau, 2000, Modelling quartz cementation and porosity in reservoir sandstones: Examples from the Norwegian continental shelf, *in* R. H. Worden and S. Morad, eds., Quartz cementation in sandstones, Oxford, United Kingdom, Blackwell Science, v. 29, p. 39 49, doi:10.1002/9781444304237.ch3.

Waugh, B., 1970, Formation of quartz overgrowths in the Penrith Sandstone (Lower Permian) of Northwest England as revealed by scanning electron microscopy: Sedimentology, v. 14, p. 309 320, doi:10.1111/j.1365 3091.1970.tb00197.x.

Wygrala, B. P., 1989, Integrated study of an oil field in the southern Po basin, northern Italy: Jülich, Germany, Kernforschungsanlage Jülich Reports 2313, p. 217.

Ziegler, P. A., 1990, Geological atlas of Western and Central Europe: The Hague, Netherlands, Shell Internationale Petroleum Maatschapij B.V., 239 p.

Zwingmann, H., N. Clauer, and R. Gaupp, 1998, Timing of fluid flow in a sandstone reservoir of the north german Rotliegend (Permian) by K Ar dating of related hydrothermal illite, *in* J. Parnell, ed., Dating and duration of fluid flow and fluid rock interaction: Geological Society, London, Special Publications 1998, v. 144, p. 91 106, doi:10.1144/GSL.SP.1998.144.01.07.

Zwingmann, H., N. Clauer, and R. Gaupp, 1999, Structure related geochemical (REE) and isotopic (K Ar, Rb Sr, d18O) characteristics of clay minerals from Rotliegend sandstone reservoirs (Permian, northern Germany): Geochimica et Cosmochimica Acta, v. 63, p. 2805 2823, doi:10.1016/S0016 7037(99)00198 2.